Available online at www.sciencedirect.com
SCIENCE DIRECT®
PERGAMON
Journal of Asian Earth Sciences 22 (2004) 517–527
Journal of Asian Earth Sciences
www.elsevier.com/locate/jseaes

Clinopyroxene phenocrysts (with green salite cores) in trachybasalts: implications for two magma chambers under the Kokchetav UHP massif, North Kazakhstan

Yongfeng Zhu[a,b,*], Yoshihide Ogasawara[b]

[a]*The Key Laboratory of Orogenic Belts and Crustal Evolution, School of Earth and Space Sciences, Peking University, Beijing 100871, People's Republic of China*
[b]*Department of Earth Sciences, Waseda University, Tokyo 169-8050, Japan*

Received 19 April 2002; revised 13 September 2002; accepted 20 February 2003

Abstract

Clinopyroxene phenocrysts in the Kokchetav trachybasalts are variable in composition and textures. Two distinctive cores are recognized: diopside cores and green salite cores. The diopside cores with Mg# of 80–90 are mantled by colorless salite rims with Mg# of 70–80. The green salite cores have especially low Mg# (<70) but high Al and Ti contents. A Mg-rich band (Mg# = 82–90) usually occurs between a green salite core and its rim, and/or between a colorless salite mantle and its rim. Dissolution surfaces are observed on all textural variants. Two magma chambers are needed to explain the observed clinopyroxene phenocrysts. A deep chamber at about 120 km in the upper mantle in which diopside cores crystallized, and a shallow chamber at depths of less than 40 km in which diopside cores were resorbed and overgrown by salite rims or mantles. Magma mixing in the shallow chamber is responsible for the formation of dissolution surfaces between the diopside bands and the colorless salite mantles. The dissolution surfaces on the diopside cores formed in the shallow chamber as a result of pressure decrease. This magma evolution scenario is complicated by the occurrence of the crustal-origin green salite cores in diopsides. These green cores likely represent the relics of continental materials, which were captured in the deep chamber and partially re-melted. Our observations indicate that subducted continental materials were returned to the Earth's surface as a result of magmatism. This study therefore provides direct evidence of a link between subducted continental materials (slab) and magmatism in this orogenic belt.

Keywords: Kokchetav; Trachybasalt; Clinopyroxene; Salite; Magma mixing; Subduction

1. Introduction

Chemical zonation in clinopyroxene phenocrysts records magmatic histories. Such zonation may form due to varying mineral-melt equilibria for phenocrysts growing in magmas that are evolving by fractional crystallization, or it may be produced by crystal chemistry or by the kinetics of crystal growth (Shimizu, 1990). Many investigators have confirmed that the continuous and discontinuous, normal and inverse chemical zonations of clinopyroxenes in mafic rocks record complex patterns for the evolution of magmas, involving several batches of magma and various intermediate evolutionary stages under different physico-chemical conditions (Markl and White, 1999). For example, clinopyroxene xenocrysts record a high-pressure stage of crystallization of alkali basaltic magma (Wilkinson, 1975; Wass, 1979; Irving and Frey, 1984); they may also represent an early liquidus phase in equilibrium with the host liquid at high pressures in the upper mantle (Dobosi, 1989). Three types of clinopyroxene megacrysts have been identified in lavas of West Eifel, Germany (Shaw and Eyzaguirre, 2000), which were derived from three different batches of magma: magnesium-rich magma in the lithospheric mantle; moderately magnesium-rich magmas in the lithospheric mantle and possibly in the lower crust, and iron-rich magma in the middle to lower crust.

Clinopyroxenes with normal and continuous major element zonation generally indicate relatively simple growth histories (Kay and Kay, 1985; Singer et al., 1992).

* Corresponding author. Address: The Key Laboratory of Orogenic Belts and Crustal Evolution, School of Earth and Space Sciences, Peking University, Beijing 100871, People's Republic of China.
E-mail address: yfzhu@pku.edu.cn (Y. Zhu).

1367-9120/03/$ - see front matter © 2003 Elsevier Ltd. All rights reserved.
doi:10.1016/S1367-9120(03)00091-9

Reversed major element zonation in clinopyroxene, however, implies that the magma evolved in an open system prior to eruption such as the reaction between a silicic melt and peridotite in the upper mantle (Kay, 1978; Myers et al., 1985; Myers and Frost, 1994) and/or the mixing of a silicic melt and a primitive basaltic melt (Yogodzinski et al., 1995). In this manuscript, we describe different kinds of clinopyroxene phenocrysts in the Kokchetav trachybasalts, and discuss magmatic processes that likely relate to the recycling of subducted continental materials. Such processes are essential for the formation of the Central Asian orogenic belt, which is formed dominantly from subduction-accretion and migration of the original magmatic-arc axis towards the ocean in episodic jumps. These Altaid-type collages add considerable amounts of juvenile crust to the continents (Sengor and Natal'in, 1996). We interpret the green salite cores found in diopside phenocrysts as crustal-origin xenoliths, which were recycled to the upper mantle and partially melted at depths >120 km. Future laser-ablation $^{16}O/^{18}O$ measurements on such salite xenoliths may provide more information to support the hypothesized recycling process of continental materials in this region.

2. Geological background

The huge Central Asian orogenic belt consists of the Altaids on the north and Manchurides on the south (Sengor and Natal'in, 1996). The Altaids consists of five units (from east to west): Mongol-Okhotsk orogen, the Altai/Sayan orogen, the Kazakhstan folded region, the Tianshan orogen, and the Ural orogen. The Kokchetav Precambrian block consists of various porphyroids, schists, amphibolites, phyllites, marbles, and dolomites. Unconformably overlying the Vendian–Cambrian diamictites are basalts, rhyolites, rare andesite-basalts, and volcaniclastic rocks that are intruded by ultramafic–mafic layered plutons. Cambrian shallow-marine carbonates, shales, and sandstone, Middle Ordovician clastics, Upper Ordovician tuffs, conglomerates, and intermediate volcanics, together with vast granodiorites indicate a long-lived magmatic arc (Sengor and Natal'in, 1996). The diamond-bearing Kokchetav metamorphic massif is located in the northern part of the Kazakhstan folded region. Diamond- and coesite-bearing rocks have been found among Precambrian gneisses, granite-gneisses, schists, granulites, amphibolites, quartzites, marbles, and eclogites (Sobolev and Shatsky, 1990). Metamorphism of the diamond-bearing parageneses took place in the Middle Cambrian, as indicated by U–Pb (Claoue-Long et al., 1991) and Sm–Nd (Shatsky et al., 1999) ages of 520–540 Ma. These ultrahigh pressure (UHP) metamorphic rocks were covered by Devonian volcanic rocks and Carboniferous and Triassic shallow-water and lacustrine deposits (Dobretsov et al., 1995), and intruded by Silurian to Early Devonian granites and Late Devonian to Carboniferous granitic rocks.

Four lithologic units have been identified in the Kokchetav UHP massif (Kaneko et al., 2002). Unit I, the lowermost structurally, consists mainly of amphibolite and acid schist lenses or layers. This unit mainly crops out in the western part of the Kokchetav UHP massif and is tectonically overlain by the UHP rocks of Unit II. Unit II is composed mainly of gneiss and white schist that contain eclogite blocks. Diamonds occur as inclusions in garnet and zircon in the pelitic gneiss and white schist in the Kumdy-Kol region of the west Kokchetav UHP massif. The Kumdy-Kol accretionary complex is comprised of Vendian to Ordovician ophiolites, pelagic cherts, and turbidites invaded by the migrating late Ordovician magmatic front (Ivanov et al., 1988). Unit III is predominantly composed of amphibolite and gneiss. This unit contains minor eclogite lenses. No diamond inclusions are found in this unit. Units III and II, which are covered by the rocks of Unit IV, mainly consists of pelitic–psammitic schist and gneiss. The boundaries between these lithologic units usually are faults. Units II and III occupy a large area in the Borovoye region east of the Kokchetav UHP massif, where the studied volcanic rocks crop out (Fig. 1(b)). This region, however, lacks rocks of unit I. The rocks of unit III are concentrated in the center of unit II. Unit IV directly covers unit II. Volcanic rocks lie on top of gneiss and eclogite-bearing white schist.

3. Petrography of the volcanic rocks

Volcanic rocks consisting mainly of tuff breccia and welded tuff are distributed in the Borovoye uplift region, along the north shores of Small Chebachye Lake and Big Chebachye Lake, where they unconformably cover gneiss (containing abundant amphibolite lenses) and eclogite-bearing white schist in the north, and amphibolite-free gneiss to the south (Fig. 1(b)). The latter was intruded by the Devonian granitic rocks. Faults mark the contact boundaries between the volcanic rocks and their country rocks. The volcanic rocks extend more than 13 km in a NEE-direction with an outcrop area of about 10 km^2. The volcanic sequences are not clear due to poor outcrop. The age of these volcanic rocks is unknown, and it is unknown whether these volcanic rocks are related to the Devonian volcanic rocks described by Dobretsov et al. (1995). Field surveys only revealed that they covered the UHP metamorphic rocks, which implies that the volcanism is younger than 540 Ma, and therefore could be related to post-collisional magmatism in the newly assembled Asian continent (Sengor and Natal'in, 1996).

Two different volcanic rock types have been recognized based on whole-rock chemical analysis (Zhu et al., 2002): trachybasalt and basaltic trachyandesite, both belonging to the shoshonitic group with high-K contents (2.9–6.2 wt% K_2O). These two distinct rocks also differ in their mineral assemblages. The trachybasalts mainly consist of clinopyroxene phenocrysts (>30 vol%) with

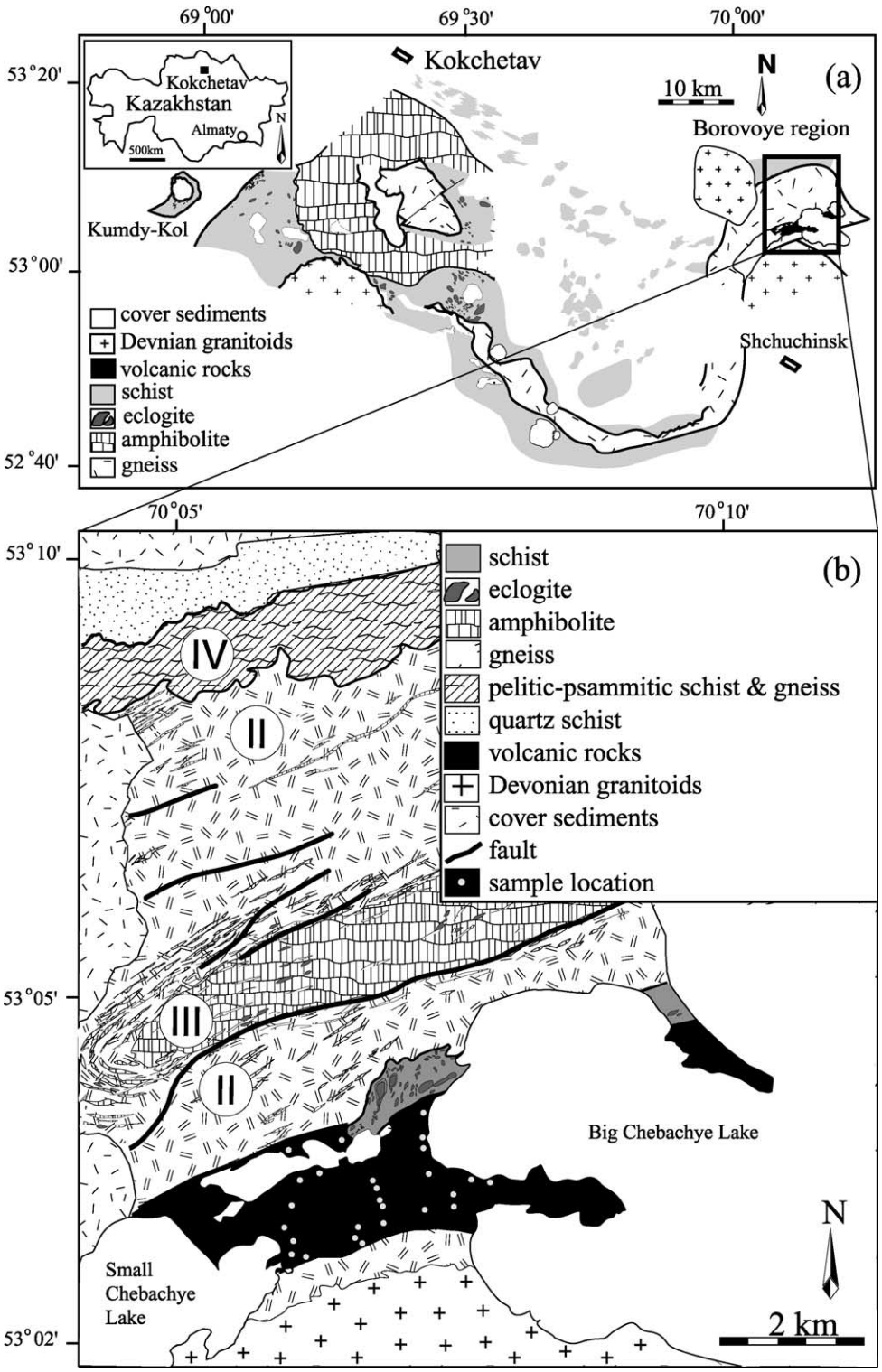

Fig. 1. (a) A simplified geological map for the Kokchetav Massif; (b) geological map of the Borovoye region, where volcanic rocks crop out. II–IV correspond to the lithologic units of the UHP massif (modified from Kaneko et al. (2002), see text for details).

minor phlogopite–biotite (<2%) and magnetite (about 1%) phenocrysts; the fine-grained groundmass consists of sanidine and albite with minor amounts of magnetite and biotite. Actinolite occurs in the groundmass, and in rare cases, replaces clinopyroxene phenocrysts along the rims. The basaltic trachyandesites contain plagioclase (<5 vol%, An <25) and sanidine (<10%) phenocrysts as well as clinopyroxene phenocrysts (10–20%). The clinopyroxene phenocrysts in trachyandesites are relatively simple in texture (continuous growth) compared

with the trachybasalts (discontinuous growth). Here we only focus on the discontinuous growth processes of the clinopyroxene phenocrysts from the trachybasalts.

Almost all clinopyroxene phenocrysts (mainly 0.1–0.6 mm and rarely up to 1.5 mm in length) in trachybasalts have core–rim textures with rounded cores and thin rims (Fig. 2(a)). Some clinopyroxene cores are irregular in shape and seem to have undergone resorption before the growth of their rims (Fig. 2(b) and (c)). In some cases, the clinopyroxene phenocryst is complexly zoned with a rounded core, a wide mantle, an irregular band, and a thin rim (Fig. 2(d)). A kind of green core, which is found in a few clinopyroxene phenocrysts, is heterogeneous in composition and elliptical in shape (Fig. 2(e) and (f)). All these different clinopyroxene phenocrysts coexist in trachybasalts based on the observation of 43 thin-sections from 31 samples covering most of the outcrop area of the Kokchetav volcanic rocks (see Fig. 1(b)).

4. Methods of analysis

Mineral analyses were carried out by wavelength dispersion (WDS) X-ray spectrometry on a JEOL Superprobe 8900 electron microprobe installed at Waseda University. Use of a LaB_6 filament ensured stable working conditions. The operation conditions were set to 15 kV and 20 nA using a beam defocused to 10 μm for point analysis. Counting times were 100 s per element. Natural minerals and synthetic pure oxides were used as standards. Precision is better than 1% for element oxides. Representative analyses of clinopyroxene are reported in Table 1. X-ray mapping was performed in order to reveal the compositional texture of complexly zoned clinopyroxene crystals. The beam duration for each point is 20–30 ms.

5. Results

Over 300 analyses were performed on 28 representative clinopyroxene phenocrysts from trachybasalts, and the results are shown in plots of Wo–En–Fs (Fig. 3(a)) and Al_2O_3 versus TiO_2 (Fig. 3(b)). The compositions of clinopyroxene phenocrysts with green cores are distinct from those with colorless cores. The green cores are salite in composition and are characterized by high Wo (up to 51 mol%) and Fs contents (>11 mol%), which contain high Al_2O_3 (3.7–7.0 wt%) and TiO_2 (0.60–1.25 wt%). In contrast, the colorless cores in clinopyroxene phenocrysts are mainly diopside and have low Al_2O_3 (<3.0 wt%) and TiO_2 (<0.6 wt%) contents. The rims of clinopyroxene phenocrysts are totally salite and contain higher Al_2O_3 and TiO_2 relative to the colorless cores. The rims partially overlap the green cores, especially in the Al_2O_3–TiO_2 plot (Fig. 3(b)). The bands in some clinopyroxene phenocrysts are similar to the colorless cores and plot in diopside field in the Wo–En–Fs plot, and between the diopside cores and salite rims in the Al_2O_3–TiO_2 plot. The mantles, however, are similar to the rims, and plot in the salite field in the Wo–En–Fs plot, and between the diopside cores and salite rims in the Al_2O_3–TiO_2 plot. Therefore, three different clinopyroxenes can be distinguished: (1) the green salite cores; (2) the colorless diopside cores and the diopside bands; (3) the colorless salite mantles and rims. Although the mantles and the rims are both classified here as colorless salite, their compositions are different in trace elements such as Al and Ti as shown in Fig. 3(b). The rims contain higher Al and Ti relative to the mantles. This probably reflects the difference of their crystallization environments, as the mantles obviously crystallized before the rims and the bands.

Most clinopyroxene phenocrysts in the Kokchetav trachybasalts are chemically zoned with a diopside core and a salite rim as shown in Fig. 2(a). The core is higher in Mg# (80–90) and Si but lower in Al contents relative to its rim (Fig. 4(a), (d) and (g)). The compositional profile of this crystal is typical of clinopyroxene phenocrysts with diopside cores and salite rims. The clinopyroxene phenocrysts with irregular diopside cores as shown in Fig. 2(b) and (c) also have similar compositional profiles.

The clinopyroxene phenocryst with a complex texture consisting of core, mantle, band and rim (Fig. 2(d)) usually shows a dissolution surface on its diopside core and salite mantle, respectively. The band between the resorbed mantle and the rim varies in width from several micrometers up to 30 μm. Its outer outline shows an euhedral crystal shape. Similar to its core, the band is Mg-rich and Al-poor relative to rim and mantle (Fig. 4(b) and (e)), and there is a compositional gap between the core and the mantle, between the mantle and the band, as well as between the band and the rim (Fig. 4(h)).

The green cores in clinopyroxene phenocrysts are heterogeneous in composition, and are characterized by low Mg concentrations (Fig. 4(c)) and low Si but high Al contents (Fig. 4(f)) relative to their margins. The boundary (band) between the green cores and their margins are characterized by higher Mg and Si but lower Al contents. The drastic change in composition between the band and the green core (Fig. 4(i)) implies that the band did not crystallize from the same magma from which the green core formed.

6. Discussion

6.1. The green core—xenocryst of continental origin?

Clinopyroxene phenocrysts with different compositions and structures usually reflect original magmatic differences (Bindi et al., 1999). The green cores in clinopyroxene phenocrysts from the Kokchetav trachybasalts generally have a rounded outline, and are compositionally unlike any of the other clinopyroxenes in the same rocks. In addition to being relatively Fe-rich, the green cores contain significantly higher

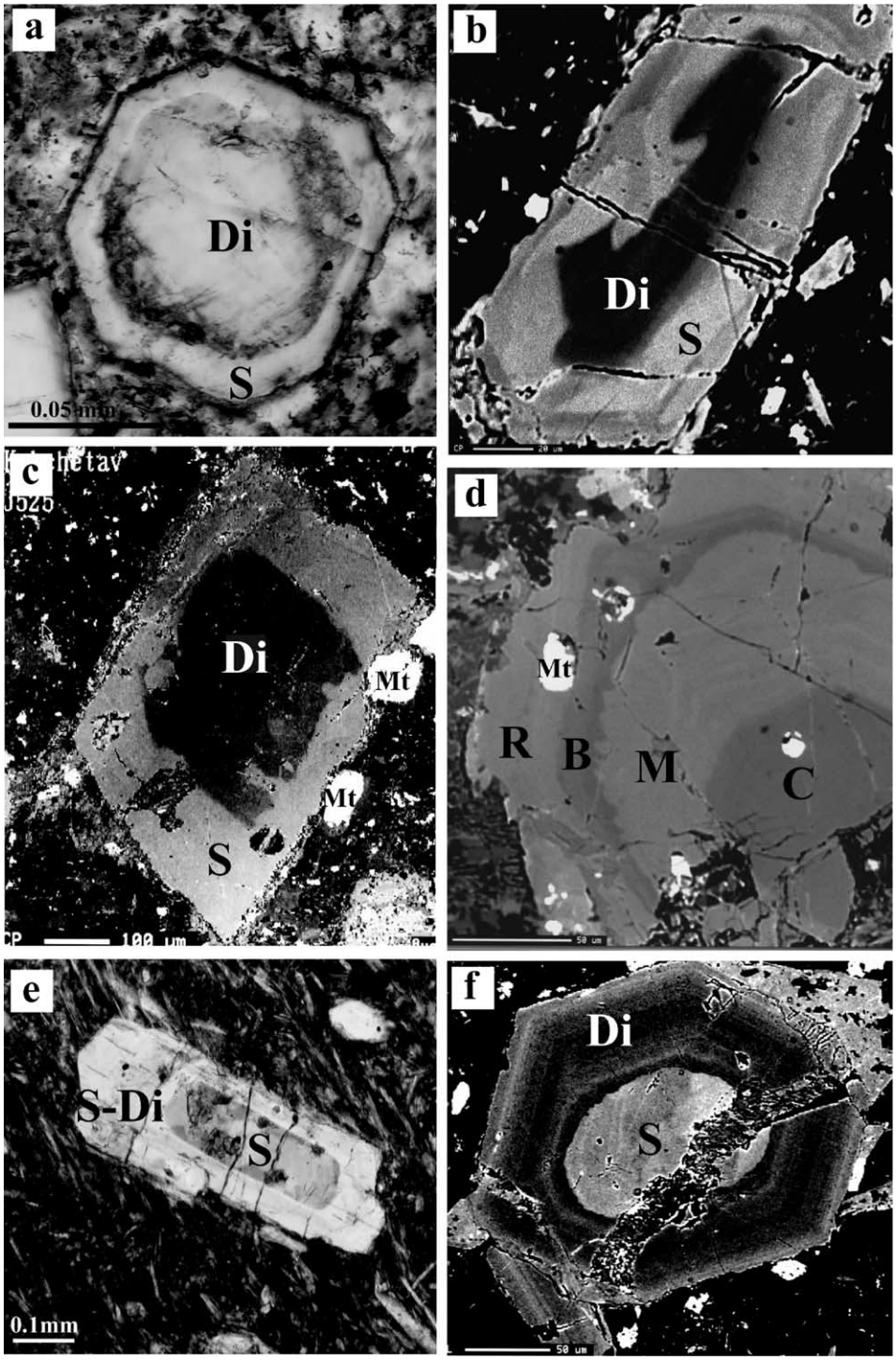

Fig. 2. Photomicrographs of clinopyroxene phenocrysts in the Kokchetav trachybasalts: (a) an euhedral clinopyroxene phenocryst with a core–rim texture, plane-polarized light, scale bar = 50 μm; (b) a clinopyroxene phenocryst with an irregular and resorbed diopside core, X-ray image, scale bar = 20 μm; (c) an embayed diopside core is surrounded by the salite rim, which contacts with magnetite (white) in the groundmass, X-ray image, scale bar = 100 μm; (d) a broken phenocryst with a rounded diopside core (C), a resorped mantle (M), a diopside band (B), and a salite rim (R). Magnetite (white) occurs as inclusions on the boundary between the band and rim, X-ray image, scale bar = 50 μm; (e) a clinopyroxene phenocryst with a green core, crossed-polars, scale bar = 100 μm; (f) the X-ray image of a clinopyroxene phenocryst with a green core, scale bar = 50 μm. Di, diopside; S, salite; Mt, magnetite.

levels of Al_2O_3 and TiO_2 (Fig. 3(b)). Wide compositional variations occur inside one grain and no systematic zonation pattern is evident, but the green cores from different phenocrysts have similar textures and compositions.

Green clinopyroxenes of broadly similar composition have been described from a wide variety of alkaline rocks (Thompson, 1977). The aluminum-rich (>5.0 wt% Al_2O_3) salite cores have been described from the pillow lavas and

Table 1
Representative composition of clinopyroxene phenocrysts from the Kokchetav trachybasalts

Oxides (wt%)	Green core	Green core	Green core	Green core	Green core	Green core	Green core	Green core	Di core	Di core	Di core	Di core	Di core	Di core	Di core	Di core	Di core	Di core	Di core
SiO_2	48.79	49.4	47.31	47.37	46.09	45.86	49.87	49.95	52.72	53.01	53.88	53.02	52.95	52.71	52.38	52.07	53.78	53.58	53.41
TiO_2	0.63	0.62	1.03	0.92	1.24	1.16	0.60	0.59	0.11	0.21	0.19	0.26	0.59	0.42	0.50	0.51	0.15	0.16	0.18
Al_2O_3	4.41	4.04	6.38	5.92	6.95	6.92	3.73	3.72	1.58	1.30	0.87	1.54	2.75	2.65	2.77	3.09	0.78	0.95	1.10
MgO	11.78	11.62	10.32	11.44	10.18	9.98	11.68	11.78	15.79	16.61	17.18	16.17	15.82	15.96	15.53	14.78	17.15	17.51	16.94
MnO	0.20	0.16	0.14	0.12	0.20	0.10	0.30	0.24	0.11	0.11	0.12	0.12	0	0.08	0.12	0.07	0.20	0.21	0.20
FeO	9.40	9.43	10.26	9.72	10.98	11.40	9.57	9.10	4.25	3.66	3.29	3.63	5.68	5.53	5.64	6.38	3.26	3.08	3.27
Cr_2O_3	0	0.01	0.01	0	0	0.02	0	0.02	0.44	0.34	0.44	0.65	0.13	0.21	0.09	0.04	0.23	0.40	0.43
CaO	23.64	23.70	23.41	23.70	23.61	23.66	23.24	23.55	23.95	23.8	23.51	23.77	21.75	23.05	22.52	22.73	23.66	23.31	23.48
Na_2O	0.27	0.25	0.42	0.21	0.27	0.28	0.25	0.27	0.32	0.18	0.08	0.16	0.14	0.14	0.16	0.17	0.09	0.07	0.14
K_2O	0.02	0	0.03	0.01	0	0.01	0	0	0	0	0	0	0.01	0.01	0	0	0.02	0	0
Total	99.13	99.23	99.30	99.41	99.52	99.40	99.23	99.21	99.26	99.22	99.55	99.31	99.82	100.76	99.71	99.84	99.33	99.26	99.14
Apfu (O = 6)																			
Si	1.856	1.876	1.803	1.803	1.766	1.763	1.891	1.891	1.949	1.954	1.973	1.953	1.941	1.924	1.930	1.923	1.975	1.967	1.965
Ti	0.018	0.018	0.029	0.026	0.036	0.034	0.017	0.017	0.003	0.006	0.005	0.007	0.016	0.012	0.014	0.014	0.004	0.004	0.005
Al^{IV}	0.144	0.124	0.197	0.197	0.234	0.237	0.109	0.109	0.051	0.046	0.027	0.047	0.059	0.076	0.070	0.077	0.025	0.033	0.035
Al^{VI}	0.053	0.056	0.090	0.068	0.079	0.076	0.057	0.057	0.017	0.011	0.01	0.019	0.060	0.038	0.050	0.057	0.008	0.008	0.013
Mg	0.667	0.657	0.586	0.648	0.581	0.572	0.659	0.664	0.869	0.911	0.937	0.886	0.864	0.867	0.852	0.813	0.937	0.957	0.928
Mn	0.006	0.005	0.005	0.004	0.006	0.003	0.010	0.008	0.003	0.004	0.004	0.004	0	0.002	0.004	0.002	0.006	0.006	0.006
Fe	0.298	0.298	0.326	0.308	0.351	0.365	0.302	0.287	0.131	0.112	0.100	0.111	0.174	0.168	0.173	0.196	0.100	0.094	0.100
Cr	0	0	0	0	0	0.001	0	0.001	0.013	0.010	0.013	0.019	0.004	0.006	0.003	0.001	0.007	0.011	0.012
Ca	0.964	0.964	0.956	0.967	0.969	0.975	0.944	0.955	0.948	0.940	0.922	0.938	0.854	0.902	0.889	0.899	0.931	0.917	0.925
Na	0.020	0.018	0.031	0.016	0.020	0.021	0.019	0.020	0.023	0.013	0.006	0.011	0.010	0.010	0.012	0.012	0.007	0.005	0.010
K	0.001	0	0.001	0.001	0	0	0	0	0	0	0	0	0	0.001	0	0	0.001	0	0
Total	4.027	4.017	4.024	4.038	4.042	4.046	4.009	4.009	4.008	4.007	3.997	3.997	3.981	4.005	3.995	3.995	4.001	4.003	4.000
Mg#[a]	68.7	68.4	63.9	67.5	61.9	60.8	67.9	69.2	86.6	88.7	90.0	88.5	83.3	83.6	82.8	80.4	89.9	90.5	89.7
Oxides (wt%)	Band	Band	Band	Band	Band	Band	Mantle	Mantle	Mantle	Mantle	Mantle	Mantle	Rim	Rim	Rim	Rim	Rim	Rim	Rim
SiO_2	52.56	52.43	53.00	53.09	53.48	51.88	50.58	51.63	51.28	48.29	48.71	49.92	51.36	51.57	51.17	50.56	50.22	49.9	49.93
TiO_2	0.42	0.29	0.28	0.24	0.47	0.49	0.71	0.62	0.54	0.68	0.69	0.63	0.49	0.59	0.55	0.52	0.66	0.59	0.65
Al_2O_3	1.89	1.88	1.53	1.47	2.18	2.47	3.93	3.13	3.44	3.70	4.95	4.68	3.06	3.01	2.90	3.63	3.72	4.15	4.26
MgO	15.37	16.17	16.66	16.26	15.8	15.37	14.08	15.20	13.81	13.47	11.98	12.49	14.26	14.57	14.24	14.05	13.95	13.70	13.41
MnO	0.16	0.15	0.16	0.12	0.13	0.2	0.21	0.19	0.11	0.16	0.28	0.31	0.12	0.13	0.09	0.17	0.17	0.20	0.28
FeO	5.37	4.56	3.40	3.88	4.72	5.98	7.92	7.15	7.60	7.79	9.64	9.67	6.88	6.88	7.11	7.52	7.49	7.60	8.45
Cr_2O_3	0.03	0.16	0.31	0.41	0.09	0.07	0	0.06	0	0	0	0.02	0.01	0.02	0	0	0.07	0	0
CaO	23.91	23.48	23.84	23.9	23.39	23.55	22.18	22.48	22.22	22.36	23.42	22.92	23.41	23.32	23.15	22.68	22.80	23.09	23.09
Na_2O	0.14	0.14	0.15	0.13	0.14	0.18	0.17	0.16	0.14	0.19	0.18	0.18	0.24	0.22	0.18	0.22	0.18	0.26	0.18
K_2O	0	0	0	0.01	0	0.05	0	0	0	0.01	0.05	0.05	0.01	0	0	0	0	0	0.05
Total	99.85	99.26	99.33	99.50	100.40	100.23	99.77	100.61	99.15	96.64	99.90	100.88	99.84	100.31	99.38	99.34	99.27	99.49	100.31
Apfu (O = 6)																			
Si	1.941	1.939	1.950	1.954	1.950	1.914	1.885	1.902	1.917	1.868	1.840	1.861	1.908	1.906	1.911	1.892	1.883	1.869	1.864
Ti	0.012	0.008	0.008	0.007	0.013	0.014	0.020	0.017	0.015	0.020	0.020	0.018	0.014	0.016	0.015	0.015	0.019	0.017	0.018
Al^{IV}	0.059	0.061	0.050	0.046	0.050	0.086	0.115	0.098	0.083	0.132	0.160	0.139	0.092	0.094	0.089	0.108	0.117	0.131	0.136
Al^{VI}	0.023	0.021	0.016	0.017	0.044	0.021	0.058	0.037	0.068	0.036	0.060	0.066	0.042	0.037	0.039	0.052	0.047	0.052	0.050
Mg	0.845	0.890	0.912	0.891	0.858	0.844	0.781	0.834	0.769	0.775	0.674	0.693	0.789	0.802	0.792	0.783	0.779	0.764	0.745
Mn	0.005	0.005	0.005	0.004	0.004	0.006	0.006	0.006	0.003	0.005	0.009	0.010	0.004	0.004	0.003	0.005	0.005	0.006	0.009
Fe	0.165	0.141	0.104	0.119	0.143	0.184	0.246	0.219	0.237	0.251	0.304	0.301	0.213	0.212	0.221	0.234	0.234	0.237	0.263
Cr	0.001	0.005	0.009	0.012	0.003	0.002	0	0.002	0	0	0	0.001	0	0.001	0	0	0.002	0	0
Ca	0.946	0.930	0.940	0.942	0.914	0.931	0.886	0.887	0.890	0.927	0.948	0.915	0.932	0.924	0.926	0.909	0.916	0.927	0.923
Na	0.010	0.010	0.011	0.009	0.010	0.013	0.012	0.011	0.010	0.014	0.013	0.013	0.017	0.016	0.013	0.016	0.013	0.019	0.013
K	0	0	0	0	0	0.002	0	0	0	0	0.002	0.002	0.001	0	0	0	0	0	0.002
Total	4.006	4.009	4.005	4.002	3.989	4.017	4.009	4.013	3.992	4.028	4.030	4.019	4.011	4.012	4.01	4.014	4.015	4.022	4.025
Mg#[a]	83.2	86.0	89.3	87.9	85.3	81.6	75.6	78.7	76.2	75.2	68.3	69.1	78.4	78.8	77.9	76.6	76.5	75.8	73.3

[a] $Mg\# = 100Mg/(Fe + Mn + Mg)$.

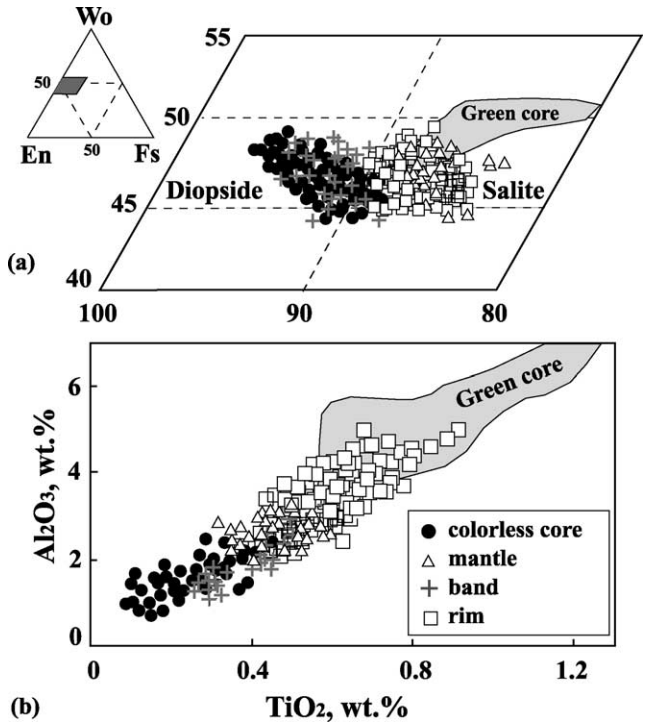

Fig. 3. An En–Wo–Fs diagram (a) and Al_2O_3–TiO_2 plot (b) showing the compositions of clinopyroxene phenocrysts from the Kokchetav trachybasalts. The shaded area corresponds to the compositional space of the green cores in clinopyroxene phenocrysts from the same rocks.

sills of the Karawanken Mountains of southeast Austria (Loeschke, 1973), from the leucite tephrites of Vesuvius, the phonolitic tephrites of Monte Somma (Rahman, 1975), and from the feldspar-free melitite and melafoidite of Monte Vulture, Italy (Bindi et al., 1999). Salite is also the common microphenocrystal phase in leucite-bearing lavas in the northern part of the Roman volcanic region (Cundari, 1975). The interpretation of such green cores in clinopyroxene phenocrysts is rather controversial. Wass (1979) suggested that the Fe-rich clinopyroxene core represents a product of a high-pressure differentiation. Barton and Bergen (1981), however, ruled out a high-pressure cognate relationship, as it is impossible for salite to crystallize from a Mg-rich magma such as its current host diopside. Such Fe-rich clinopyroxene cores are thought to represent either wall-rock debris entrained by the rising magma (Barton and Bergen, 1981) or to be a product of crystallization of an evolved magma, which subsequently mixed with a more primitive magma (Duda and Schmincke, 1985). Dobosi (1989) found two different Fe-rich cores in the same alkali basalts: one is thought to represent xenocrysts derived from upper mantle rocks, the other precipitated from relatively evolved melt which has been mixed into its present host magma.

The green cores in the Kokchetav trachybasalts obviously are not formed from the relatively evolved magma from which their salite rims grew. There is a possibility that the green cores formed in the same melt from which the salite mantles crystallized as both the green cores and the mantles are salite in composition and overlap in the Al–Si plot (Fig. 4(e)). However, the large difference in Ca concentrations (Figs. 3(a) and 4(h)) and TiO_2 contents (Fig. 3(b)) rule out this possibility. These characteristics suggest that the green cores in the Kokchetav clinopyroxene phenocrysts were not derived from the same magma from which the host diopside–salite formed, and imply that the green cores were introduced as xenocrysts into magma from elsewhere (most possibly from the subducted continental materials). If the green cores come from subducted continental materials, this study provides direct observation showing the recycling of continental materials by magmatism. Such processes have been inferred from geochemical characteristics of volcanic rocks in many other regions (Liegeois et al., 1998; Zhu and Ogasawara, 2000; Zhu et al., 2001; Bourdon et al., 2002). Future measurements of $^{16}O/^{18}O$ on such salite cores (in situ, by laser-ablation) may provide evidence of their origin, as clinopyroxene of crustal-origin should differ from the mantle-origin clinopyroxene in $\delta^{18}O$ values (Eiler et al., 1997; Zheng et al., 1998).

6.2. The dissolution processes

The dissolution surfaces record the discontinuity of crystal growth. Textural and chemical disequilibria in a phenocryst assemblage are commonly considered as evidence of magma mixing (O'Brien et al., 1988; Zhu, 1994; Geshi, 2000; Hansen and Gronvold, 2000; Tepley et al., 2000; Troll and Schmincke, 2002). The Mg# of the studied clinopyroxene is highly variable across the bands and dissolution surfaces. We argue that the spikes in Mg# (Fig. 4(a)–(c)) indicate the change in compositional and thermal regimes of the magma chamber due to recharge with hotter, more Mg-rich magma. Recharge magma can dramatically influence the compositional and thermal regime of the pre-existing magma.

Two patterns of dissolution occur in clinopyroxene phenocrysts from the Kokchetav trachybasalts: the dissolution of diopside cores (Fig. 2(b)–(d)) and the dissolution of salite mantles (Fig. 2(d)). Mixing with a hotter Mg-rich magma can account for the dissolutions of the salite mantles due to temperature increases and changing of magma composition. Mg-rich clinopyroxene (generally crystallized from a primitive magma at high temperature) should not dissolve in a more evolved magma because of the lower temperature. However, such dissolutions happened in the diopside cores (Fig. 2(b)–(d)) where Mg-rich diopside was dissolved by salite. One explanation for this diopside dissolution could be a pressure decrease at a constant temperature. Magma eruption could cause a phase boundary shift, resulting in a two-stage cooling history (McCoy et al., 1992). Clinopyroxene that formed at high pressure becomes unstable at lower pressure and may be replaced by clinopyroxene of a new composition. The dissolution surfaces between the diopside cores and salite rims and

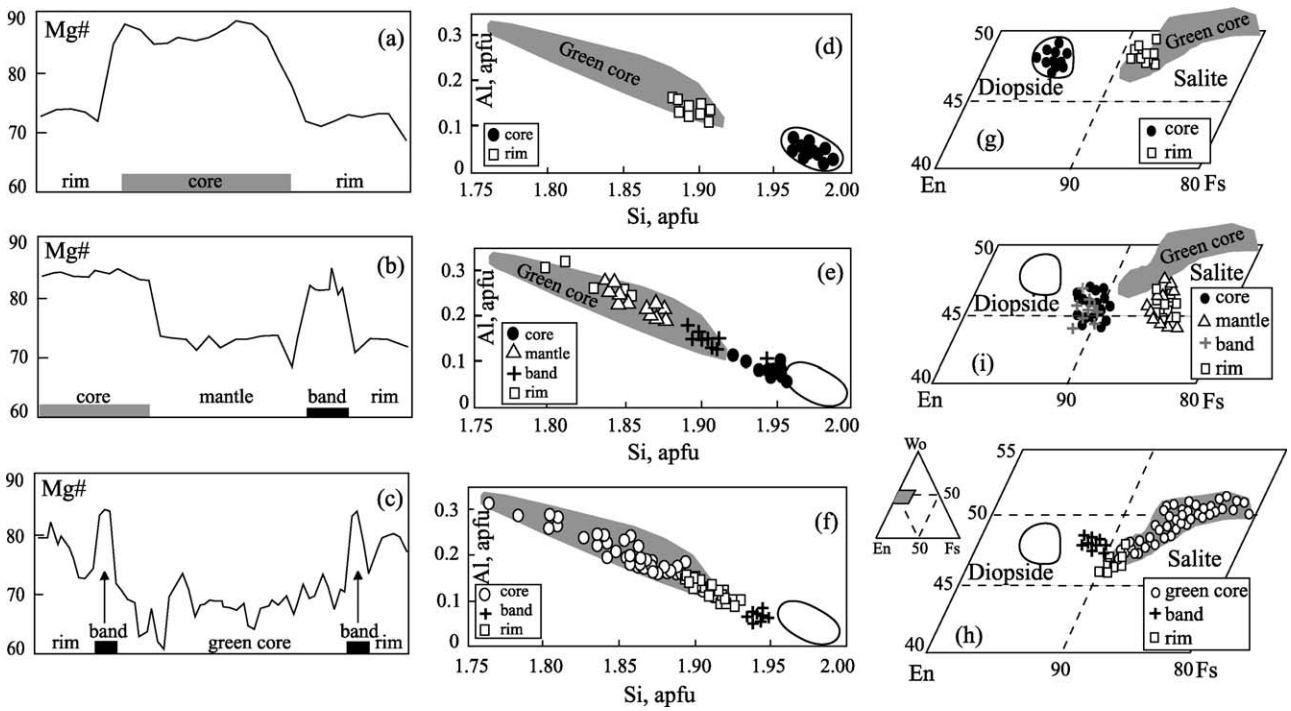

Fig. 4. Profiles across three representative clinopyroxene phenocrysts show Mg# variations (a–c). The compositional spaces for clinopyroxene phenocrysts are displayed in plots of Si versus Al contents (d–f) and Wo–En–Fs diagrams (g–i). The shaded area corresponds to the green cores. The compositional space of a primitive clinopyroxene phenocryst (the circled space) is compiled for comparison.

their compositional gap (Figs. 3 and 4) suggest that clinopyroxene cores and rims were formed in different magmas at different stages: the magma from which the diopside cores crystallized was relatively rich in Mg and formed at an early stage; the salite rims, obviously formed at a later stage and grew in a more differentiated magma. It is generally believed that Mg-rich clinopyroxene grows in primitive magma, whereas Fe-rich salite crystallizes in more differentiated magma (Deer et al., 1978).

Two magma chambers therefore are needed to explain the dissolution textures of these clinopyroxene phenocrysts. The magma chamber in which the diopside cores formed should be relatively deeper than that in which the salite rims grew. This is also evidenced by Al contents in clinopyroxene phenocrysts. The diopside cores are Al-poor relative to their rims (Table 1, Fig. 3(b)) as Al-rich clinopyroxene generally forms at lower pressures relative to Al-poor pyroxene (Foley and Venturelli, 1989; Liu et al., 2000). The Al concentration in clinopyroxene is controlled by reactions of $NaAlSi_3O_8 = NaAlSi_2O_6 + SiO_2$ (a) at high pressure (>3.5 GPa, Kushiro, 1969) and $CaAl_2Si_2O_6 = CaAl_2SiO_6 + SiO_2$ (b) at low pressure (0.5–1.2 GPa, Green, 1967). The reaction (a) could happen only at depths greater than 120 km (in a deep magma chamber), which would be recorded in the variation of Al concentrations in diopside cores. A large variation in Al_2O_3 contents in different diopside cores (0.7–3.0 wt%, Table 1 and Fig. 3b) but limited variation of Al concentration in individual diopside cores (Fig. 4(d) and (e)) implies that each diopside core grew at a single level. The core with the lowest Al content probably was not involved in reaction (a), while the core with highest Al contents grew at greater depth where reaction (a) occurred. The complete absence of plagioclase phenocrysts in the Kokchetav trachybasalts implies that plagioclase was unstable during the crystallization of clinopyroxene phenocrysts, and therefore indicates that reaction (a) occurred in the deep magma chamber. Reaction (b) occurred in the shallow (<40 km) magma chamber. As a result, the Al contents in clinopyroxenes and the SiO_2 activity in the residual magma increased. This is reflected in the mineral assemblage of the groundmass, mainly consisting of sanidine and albite.

6.3. P–T constraints

A single clinopyroxene thermobarometer designed by Nimis and Taylor (2000) can constrain the P–T conditions of magmatic Mg-rich clinopyroxene equilibrated with melt containing residual garnet in the upper mantle. We can assume that the Kokchetav trachybasalts were derived from partial melting of garnet peridotite. As shown in the above sections, the diopside cores grew at a depth of around 120 km, where the upper mantle consists mainly of garnet peridotite. The single clinopyroxene thermobarometer can therefore be used to estimate the crystallization pressures and temperatures of the studied clinopyroxene phenocrysts. The diopside cores yield higher pressures (2.3–5.3 GPa) and higher temperatures (750–1150 °C) than their rims (0.2–1.7 GPa, 710–900 °C). The core values indicate high pressures and

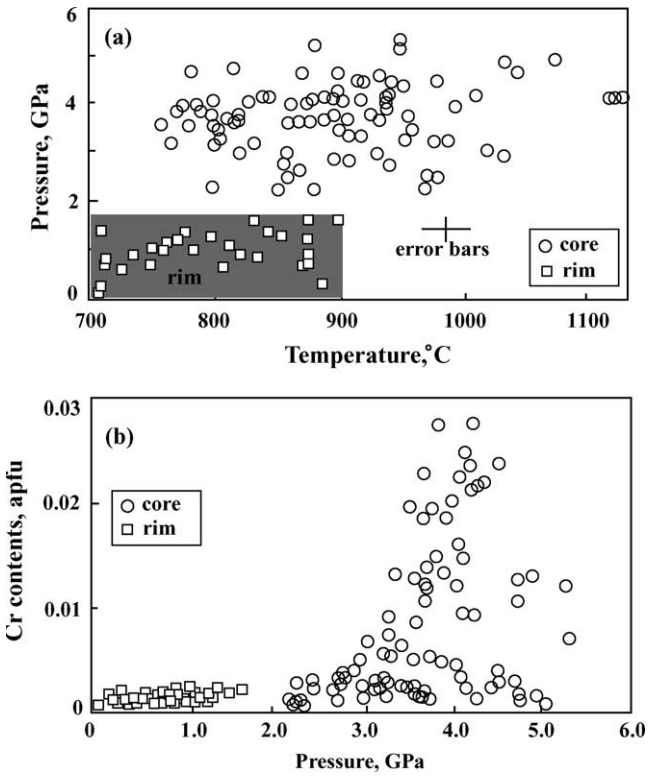

Fig. 5. (a) The calculated pressure and temperature space for clinopyroxene phenocrysts in the Kokchetav trachybasalts; (b) plots of Cr contents in clinopyroxene phenocrysts versus calculated pressure values. Note: only the analyses with Cr > 0 were used in calculations.

highly variable temperatures, whereas the rim values correspond to relatively lower and less variable temperatures and pressures (Fig. 5(a)). Taking into account the uncertainties of barometric data, pressures estimated for the diopside cores and the salite rims do not overlap. About half the temperatures of the diopside cores overlap the temperatures for the salite rims. This strongly suggests that clinopyroxene crystallization occurred in two phases (two magma chambers) for the Kokchetav trachybasalts.

The Cr contents do not correlate linearly with pressures; the highest Cr contents correspond to a pressure of ~4.0 GPa (Fig. 5(b)). Chromium is compatible and tends to partition into early crystallized mineral phases. The diopside cores, containing relatively more Cr_2O_3 than their rims, obviously served as the early crystallized phase in magma. The problem is, however, that if magma evolved in a closed system, the Cr content should decrease in the residual magma with clinopyroxene crystallization. As a result, the later stage clinopyroxene will contain less Cr. The calculated pressure values therefore reflect a magmatic differentiation trend as the thermobarometer is mainly based on the Cr contents in clinopyroxene. However, the highest values should approximate the equilibrium pressures between diopside cores in clinopyroxene phenocrysts and the residual magma.

7. Conclusions

Based on the above data and discussions, two magma chambers can be distinguished for the Kokchetav volcanic rocks. The diopside cores grew in a deep chamber at a depth of around 120 km in the upper mantle. Magma in this chamber was Mg- and Cr-rich. The crystallization of the salite rims occurred in the shallow chamber at depths less than 40 km. Magma mixed in the shallow chamber as recorded by the dissolution texture between the salite mantle and the diopside band. The differentiated magma in the shallow chamber mixed with repeated influxes of a hotter, Mg-rich magma from the deep chamber. The occurrence of a green salite core in the diopside phenocryst complicates the scenario of magma evolution, but likely provides a link between subduction and magma evolution. The crustal-origin salite core was captured in the deeper chamber. This indicates that continental materials derived from a subducted-slab returned to the Earth's surface by means of magmatism. This process therefore provides an opportunity to observe continental material recycling, which was well recorded in the UHP metamorphic rocks (Zhu and Ogasawara, 2002; Zhang et al., 2002; Zheng et al., 2003). Since this UHP massif was exhumated from depths greater than 250 km, and the studied diopside crystallized at depths of around 120 km, magma generation may have occurred at depths greater than 120 km where the green salite cores occurred as relics of continental material after partial melting.

Acknowledgements

We thank Prof. Kevin Burke (University of Houston), Jean-Paul Liegeois (Africa Museum, Belgium), and J. Noblett (Colorado College) for thorough reviews, which helped us to improve this manuscript greatly. Dr Robert Martin (McGill University) has read the early version of this manuscript and provided useful information. Prof. Y.-F. Zheng (University of Science and Technology of China) has provided some useful references. Dr J. Richards (Oregon University) revised the English exposition. This work was financially supported by the Major State Basic Research Development Program (2001CB409807) and a visiting fellowship from Waseda University to Y. Zhu.

References

Barton, M., Bergen, M.J., 1981. Green clinopyroxenes and associated phases in a potassium-rich lava from the Leucite Hills, Wyoming. Contributions to Mineralogy and Petrology 77, 101–114.

Bindi, L., Cellai, D., Melluso, L., Conticelli, S., Morra, V., Menchetti, S., 1999. Crystal chemistry of clinopyroxene from alkaline undersaturated rocks of the Monte Vulture Volcano, Italy. Lithos 46, 259–274.

Bourdon, E., Eissen, J.-P., Monzier, M., Robin, C., Martin, H., Cotton, J., Hall, M.L., 2002. Adakite-like lavas from Antisana volcano (Ecuador): evidence for slab melt metasomatism beneath the Andean northern volcanic zone. Journal of Petrology 43, 199–217.

Claoue-Long, J.C., Sobolev, N.V., Shatsky, V.S., Sobolev, A.V., 1991. Zircon response to diamond-pressure metamorphism in the Kokchetav massif, USSR. Geology 19, 710–713.

Cundari, A., 1975. Mineral chemistry and petrogenetic aspects of the Vico lavas, Roman volcanic region, Italy. Contributions to Mineralogy and Petrology 53, 129–144.

Deer, W.A., Howie, R.A., Zussman, J., 1978. Rock-Forming Minerals, 2nd ed, Single-Chain Silicates, vol. 2A. Longman, London, p. 668.

Dobosi, G., 1989. Clinopyroxene zoning patterns in the young alkali basalts of Hungany and their petrogenetic significance. Contributions to Mineralogy and Petrology 101, 112–121.

Dobretsov, N.L., Sobolev, N.V., Shatsky, V.S., Coleman, R.G., Ernst, W.G., 1995. Geotectonic evolution of diamondferous parageneses, Kokchetav Complex, Northern Kazakhstan: the geologic engima of ultrahigh-pressure crustal rocks within a Paleozoic fold belt. The Island Arc 4, 267–279.

Duda, A., Schmincke, H.U., 1985. Polybaric differentiation of alkali basaltic magmas: evidence from green-core clinopyroxenes (Eifel, FRG). Contributions to Mineralogy and Petrology 91, 340–353.

Eiler, J.M., Farley, K.A., Valley, J.W., Hauri, E., Craig, H., Hart, S.R., Stolper, E.M., 1997. Oxygen isotope variations in ocean island basalt phenocrysts. Geochimica et Cosmochimica Acta 61, 2281–2293.

Foley, S.F., Venturelli, G., 1989. High K_2O rocks with high MgO, high SiO_2 affinities. In: Crawford, A.J., (Ed.), Boninites and Related Rocks, Unwin Hyman, London, pp. 72–88.

Geshi, N., 2000. Fraction and magma mixing within intruding dike swarm: evidence from the Miocene Shitara–Otoge igneous complex, central Japan. Journal of Volcanology and Geothermal Research 98, 127–152.

Green, T.H., 1967. An experimental investigation of sub-solidus assemblages formed at high pressure in high alumina basalt, Kyanite eclogite and grosspydite compositions. Contributions to Mineralogy and Petrology 16, 84–114.

Hansen, H., Gronvold, K., 2000. Plagioclase ultraphyric basalts in Iceland: the mush of the rift. Journal of Volcanology and Geothermal Research 98, 1–32.

Irving, A.J., Frey, F.A., 1984. Trace element abundances in megacrysts and their host basalts: constraints on partition coefficients and megacryst genesis. Geochimica et Cosmochimica Acta 48, 1201–1221.

Ivanov, K.S., Sakharov, V.A., Nasedkina, V.A., Muzyka, M.I., 1988. New data on age of volcanic-siliceous formation of the Kokchetav massif rim (Northern Kazakhstan). Doklad Akademi Nauk SSSR 301, 158–163.in Russian.

Kaneko, Y., Maruyama, S., Terabayashi, M., Yamamoto, H., Ishikawa, M., Anma, R., Parkinson, C.D., Ota, T., Nakajima, M., Katayama, I., Yamamoto, J., Yamauchi, K., 2002. Geology of the Kokchetav massif. In: Parkinson, C.D., Katayama, I., Liou, J.G., Maruyama, S. (Eds.), The Diamond-Bearing Kokchetav Massif, Kazakhstan, Petrochemistry and Tectonic Evolution of an Unique Ultrahigh-Pressure Metamorphic Terrane, Universal Academy Press, Inc, Tokyo, pp. 47–70.

Kay, R.W., 1978. Aleutian magnesian andesites: melts from subducted Pacific ocean crust. Journal of Volcanology and Geothermal Research 4, 117–132.

Kay, S.M., Kay, R.W., 1985. Aleutian tholeiitic and calc-alkaline magma series I: the mafic phenocrysts. Contributions to Mineralogy and Petrology 90, 276–290.

Kushiro, I., 1969. Clinopyroxene solid solutions formed by reactions between diopside and plagioclase at high pressures. Mineralogical Society of America, Special Paper 2, 179–191.

Liegeois, J.P., Navez, J., Hertogen, J., Black, R., 1998. Contrasting origin of post-collisional high-K calc-alkaline and shoshonitic versus alkaline and peralkaline granitoids. The use of sliding normalization. Lithos 45, 1–28.

Liu, T.C., Chen, B.R., Chen, C.H., 2000. Melting experiment of a Wannienta basalt in the Kuanyinshan area, northern Taiwan, at pressure up to 2 GPa. Journal of Asian Earth Sciences 18, 519–531.

Loeschke, J., 1973. Eclogitization reactions in rocks formed at great depths. Geological Magazine 110, 19–28.

Markl, G., White, C., 1999. Complex zoning between super-calcic pigeonite and augite from the Graveyard Point sill, Oregon: a record of the interplay between bulk and interstitial liquid fractionation. Contributions to Mineralogy and Petrology 137, 170–183.

McCoy, T.J., Taylor, G.J., Keil, K., 1992. Zagami: product of a two-stage magmatic history. Geochimica et Cosmochimica Acta 56, 3571–3582.

Myers, J.D., Frost, C.D., 1994. A petrologic re-investigation of the Adak volcanic center, central Aleutian arc, Alaska. Journal of Volcanology and Geothermal Research 60, 109–146.

Myers, J.D., Marsh, B.D., Sinha, A.K., 1985. Strontium isotopic and selected trace element variations between two Aleutian volcanic centers (Adak and Atka): implications for the development of arc volcanic plumbing systems. Contributions to Mineralogy and Petrology 91, 221–234.

Nimis, P., Taylor, W.R., 2000. Single clinopyroxene thermobarometry for garnet peridotites. Part I. Calibration and testing of a Cr-in-Cpx barometer and an enstiti-in-Cpx thermometer. Contributions to Mineralogy and Petrology 139, 541–554.

O'Brien, H.E., Irving, A.J., McCallum, I.S., 1988. Complex zoning and regression of phenocrysts in mixed potassic mafic magmas of the Highwood Mountains, Montana. American Mineralogist 73, 1007–1024.

Rahman, S., 1975. Some aluminous clinopyroxenes from Vesuvius and Monte Somma. Mineralogical Magazine 40, 43–52.

Sengor, A.M.C., Natal'in, B.A., 1996. Paleotectonics of Asian: fragments of a synthesis. In: Yin, A., Harrison, T.M. (Eds.), The Tectonic Evolution of Asian, Cambridge University Press, New York, pp. 486–640.

Shatsky, V.S., Jagoutz, E., Sobolev, N.V., Kozmenko, O.A., Parkhomenko, V.S., Troesch, M., 1999. Geochemistry and age of ultrahigh pressure metamorphic rocks from the Kokchetav massif (Northern Kazakhstan). Contributions to Mineralogy and Petrology 137, 185–205.

Shaw, C.S.J., Eyzaguirre, J., 2000. Origin of megacrysts in the mafic alkaline lavas of the West Eifel volcanic field, Germany. Lithos 50, 79–95.

Shimizu, N., 1990. The oscillatory trace element zoning of augite phenocrysts. Earth Science Review 29, 27–37.

Singer, B.S., Myers, J.D., Frost, C.D., 1992. Mid-Pleistocene lavas from the Seguam Island volcanic center, central Aleutian arc: closed-system fractional crystallization of a basalt to rhyodacite eruption suite. Contributions to Mineralogy and Petrology 110, 87–112.

Sobolev, N.V., Shatsky, V.S., 1990. Diamond inclusions in garnet from metamorphic rocks: a new environment for diamond formation. Nature 343, 742–745.

Tepley, F.J. III, Davidson, J.P., Tilling, R.I., Arth, J.G., 2000. Magma mixing, recharge and eruption histories recorded in plagioclase phenocrysts from El Chichon Volcano, Mexico. Journal of Petrology 41, 1397–1411.

Thompson, R.N., 1977. Primary basalts and magma genesis: III, Alban Hills, Roman comagmatic province, Central Italy. Contributions to Mineralogy and Petrology 60, 91–108.

Troll, A.R., Schmincke, H-U., 2002. Magma mixing and crustal recycling recorded in ternary feldspar from compositionally zoned peralkaline ignimbrite 'A', Gran Canaria, Canary Islands. Journal of Petrology 43, 243–270.

Wass, S.Y., 1979. Multiple origins of clinopyroxenes in alkali basaltic rocks. Lithos 12, 115–132.

Wilkinson, J.F.G., 1975. Ultramafic inclusions and high-pressure megacrysts from a Nephelinite sill, Nandewar Mountains, northeastern New South Wales, and their nearing on the origin of certain ultramafic inclusions in alkaline volcanic rocks. Contributions to Mineralogy and Petrology 51, 235–262.

Yogodzinski, G.M., Kay, R.W., Volynets, O.N., Koloskov, A.V., Kay, S.M., 1995. Magnesian andesite in the western Aleutian Komandorsky region: implications for slab melting and processes in the mantle wedges. Bulletin of the Geological Society of America 107, 505–519.

Zhang, L.-F., Ellis, D.J., Williams, S., Jiang, W-B., 2002. Ultra-high pressure metamorphism in western Tianshan, China. Part II. Evidence from magnesite in eclogite. American Mineralogist 87, 861–866.

Zheng, Y.-F., Fu, B., Li, Y.-L., Xiao, Y.-L., Li, S.-G., 1998. Oxygen and hydrogen isotope geochemistry of ultrahigh pressure eclogites from the Dabie Mountains and the Sulu terrane. Earth and Planetary Science Letter 155, 113–129.

Zheng, Y.-F., Fu, B., Gong, B., Li, L., 2003. Stable isotope geochemistry of ultrahigh pressure metamorphic rocks from the Dabie–Sulu orogen in China: implications for geodynamics and fluid regime. Earth Science Review 1276, 1–57.

Zhu, Y.-F., 1994. Petrological significance of zoned plagioclase in Eldjurti granite and mafic microgranular enclaves, North Caucasus, Russian. Chinese Journal of Geochemistry 13, 142–155.

Zhu, Y.-F., Ogasawara, Y., 2000. The recycling of oceanic lithosphere in the Mongolia orogenic zone—evidence from the Permian volcanic rocks. EOS Transactions 81 (19), 439–440.

Zhu, Y.-F., Ogasawara, Y., 2002. Carbon recycled into the deep Earth: evidenced by dolomite dissociation in subduction-zone rocks. Geology 30, 947–950.

Zhu, Y.-F., Sun, S.-H., Gu, L.-B., Ogasawara, Y., Jiang, N., Honma, H., 2001. Perman volcanism in the Mongolian orogenic zone, northeast China: geochemistry, magma sources and petrogenesis. Geological Magazine 138, 101–115.

Zhu, Y.-F., Ogasawara, Y., Ayabe, T., 2002. The mineralogy of the Kokchetav 'lamproite': implications for the magma evolution. Journal of Volcanology and Geothermal Research 116, 35–61.